Journal of Energy Chemistry 76 (2023) 288–294

Contents lists available at ScienceDirect

Journal of Energy Chemistry

journal homepage: www.elsevier.com/locate/jechem

http://www.journals.elsevier.com/journal-of-energy-chemistry/

Improved interfacial adhesion for stable flexible inverted perovskite solar cells

Jie Dou [a,1], Qizhen Song [a,1], Yue Ma [a], Hao Wang [a], Guizhou Yuan [a], Xueyuan Wei [a], Xiuxiu Niu [a], Sai Ma [a], Xiaoyan Yang [a], Jing Dou [a], Shaocheng Liu [b], Huanping Zhou [b], Cheng Zhu [a], Yihua Chen [a], Yujing Li [a], Yang Bai [a], Qi Chen [a,*]

[a] Beijing Key Laboratory of Construction Tailorable Advanced Functional Materials and Green Applications, MIIT Key Laboratory for Low-dimensional Quantum Structure and Devices, Experimental Center of Advanced Materials, School of Materials Science and Engineering, Beijing Institute of Technology, Beijing 100081, China
[b] School of Materials Science and Engineering, Peking University, Beijing 100871, China

ARTICLE INFO

Article history:
Received 4 August 2022
Revised 16 September 2022
Accepted 27 September 2022
Available online 5 October 2022

Keywords:
ZIF-67
Flexible perovskite solar cells
Interfacial adhesion
Stability

ABSTRACT

Flexible perovskite solar cells have attracted widespread attention due to their unique advantages in lightweight, high flexibility, and easy deformation, which are suitable for portable electronics. However, the inverted (p-i-n) structured devices suffer from poor stability largely due to the low adhesion at the brittle interface (the hole transport layer/perovskite). Herein, zeolitic imidazolate framework-67 (ZIF-67) is applied to inverted structured cells to optimize the interface and prolong the device lifetime. As a result, the flexible devices based on ZIF-67 obtain the champion power conversion efficiency of 20.16%. Over 1000 h under continuous light irradiation, the device retains 96% and 80% of its original efficiency without and with bias, respectively. Notably, devices show mechanical endurance with over 78% efficiency retention after 10,000 cycles of consecutive bending cycles (R = 6 mm). The introduction of ZIF-67 suppresses the cracking in device bending, which results in improved environmental stability and bending durability.

1. Introduction

Due to the unique photoelectric properties of long carrier-diffusion length, high defect tolerance factor, absorption coefficient, and weak exciton binding energy, perovskites have attracted much scientific attention. In this decade, the certified power conversion efficiency of the rigid device has increased to 25.7% [1–4]. To commercialize perovskite solar cells (PSCs), the flexible devices with lightweight [5], high flexibility [6,7], and easy deformation [8,9], exhibit a potential market penetration for portable electronics applications [10,11]. Compared with the traditional n-i-p structure solar cells, the inverted devices with low processing temperature were suitable for flexible PSCs (f-PSCs) [12–14]. However, in the device with a p-i-n structure, the perovskite film is brittle and interacts poorly with the transport layers owing to the low adhesion [1]. The poor interface brings about increasing interface defects and is unfavorable for carrier transport, resulting in poor device efficiency and stability [15–19]. Especially in the f-PSCs, the interface between the perovskite film and the hole transport layer often causes delamination or cracking by applied stresses [20,21]. Further research efforts are required to understand the brittle interface and its effect on the environmental stability and bending durability of f-PSCs.

To date, to prolong the lifetime of flexible devices effectively, efforts have been made to improve the adhesion and optimize the properties of this interface. Reinhold H. Dauskardt's group demonstrated that the reinforcing scaffolds in perovskite solar cells could be used as a shield to protect the mechanically fragile from mechanical stresses [22]. To improve PSC efficiency and mechanical reliability, Nitin P. Padture and his colleagues created perovskite films with coarse grains to improve adhesion toughness [23]. Yuanyuan Zhou et al. enhanced the efficiency and long-term operational stability of the flexible cell by synthesizing an interpenetrating perovskite/SnO_2 interface [15]. Besides, the interfacial layer plays a role in improving the brittle interface [24–27]. To toughen the brittle interface, the iodine-terminated self-assembled monolayer [28] was reported by interlinking with the perovskite and SnO_2. The histamine diiodate [29] was also reported

* Corresponding author.
E-mail address: qic@bit.edu.cn (Q. Chen).
[1] These authors contributed equally to this work.

https://doi.org/10.1016/j.jechem.2022.09.044

to show the same effect. Although those materials could react both with the absorber and transport layers, they were only suitable for the PSCs with the n-i-p structure. Yet, there is limited research about the interlayer materials applied in flexible devices with inverted structures.

Zeolitic imidazolate frameworks (ZIFs) are stable and easily synthesized. Those materials usually contain metal ions and organo-functional groups, which could react with different types of interfaces simultaneously. During the past few years, owing to the strong coordination ability of the Co element, active N atom, and molecular configuration [30], ZIF-67 has been widely used in a variety of applications, including ion separation [31], chemical sensing [30], and catalysis [32,33]. Nevertheless, the application of ZIF-67 in the field of PSC has not been seriously explored.

Herein, we systematically investigate the interaction of ZIF-67 with the PTAA and perovskite layer. We apply ZIF-67 at the interface of the absorber and transport layer to improve the stability of the flexible device. The Co element in ZIF-67 is coordinated with the N atoms of PTAA, and simultaneously, the N atoms of ZIF-67 offer an anchor point positioned for the uncoordinated Pb^{2+} in perovskite. Therefore, it enhances the adhesion and improves the charge carrier transport at the PTAA/perovskite interface, resulting in the enhancement of the efficiency and stability of f-PSCs.

2. Results and discussion

2.1. Intermolecular interactions

To explore the interaction mechanism of ZIF-67 at the PTAA/perovskite interface, the density functional theory (DFT) calculation has been adopted. Fig. 1(a) exhibits the charge density difference of the PTAA/perovskite interface, with a threshold value of 0.001 e/$Bohr^3$. The yellow and blue colors indicate electron gain and loss, respectively, and the area evaluates the magnitude of charge. The Bader charge analysis (Fig. 1a, insert) and electron localization function (ELF) results (Fig. S1a and b, and Table S1) verify the interaction at the PTAA/perovskite interface is not strong. Due to the lack of shared electrons, the H...I or Pb...C bonding displayed a longer distance than the sum of the related atom's van der Waals radius. Hence, it clearly showed the van der Waals force dominated at the PTAA/perovskite interface. The difficulty of the interaction might be attributed to the steric hindrance, as is confirmed by the map (Fig. 1c). Within the accepted mechanism and the origin coordinates of the Pb^{2+} ion, the N element of PTAA is in a more lowland position than the benzene ring. It implies that the benzene ring of PTAA is prone to be in contact with the perovskite. In short, there was rarely chemical bonding at the PTAA/interface due to the steric hindrance.

At the brittle PTAA/perovskite interface, ZIF-67 was used to modify the interaction. As shown in Fig. 1(b), with the same threshold values, the Lewis base related to the N atom on the ZIF-67 cluster loses electrons to the undercoordinated Pb^{2+} ions. The electrophilic region associated with the Co element of the ZIF-67 cluster gains electrons from the PTAA. We quantitatively analyzed transferred charge by showing the planar average charge density difference in the x-y planes and Bader charge data (Fig. 1b, inset). The transferred charges of the PTAA/ZIF-67 cluster and ZIF-67 cluster /perovskite are about 0.14 e and 0.15 e, respectively. Both of them are much higher than the charges at perovskite/PTAA. Hence, we assumed that the ZIF-67 cluster bonded with the PTAA or perovskite layer. Fig. S1(c and d), and Table S1 revealed that the distance of Pb-N, Co-C, and Co-N bonds was short, indicative of covalent linkages. With the origin coordinates of the Pb^{2+} ion, the N element of the ZIF-67 cluster is in a protruding position in Fig. 1(d). Fig. 1(e) reveals the steric map of the ZIF-67/PTAA interfaces with the origin coordinates of the Co element. The N element of PTAA was closer than the benzene ring due to the structure of the ZIF-67 cluster, which suggested the ZIF-67 cluster was easier to contact with the N element of PTAA. We speculated that the ZIF-67 cluster, featuring a tenon and mortise structure, might exist in the interface layer and toughen the connection between the PTAA and perovskite film. The Partial Density of State (PDOS, Fig. S1e and f) analysis infers that the Co-3*d* and N-2*p* orbitals have hybridization. A strong hybridization between Pb-6s and N-2*p* orbitals at the valence-band edge is also observed. Those results revealed that the ZIF-67 cluster is beneficial for efficient charge transport at the interface [34–36]. Importantly, due to this chemical interaction, the adhesion energy of the ZIF-67 surface with PTAA and perovskite was calculated to be about 0.116 J m^{-2} and 0.060 J m^{-2}, which was several times higher than at the PTAA/ZIF-67 interface. The higher adhesion was on account of the better interface connection to improve the interfacial property of PTAA/perovskite.

Besides the theoretical calculations, we also obtained the experimental results, which are in agreement. As shown in Fig. S2, the time-of-flight secondary ion mass spectrometry (TOF-SIMS) profile displayed the distribution of the Sn^{2+}, In^{2+} MA^{+}, FA^{+}, Cs^{+}, Pb^{2+}, and Co^{2+} for the whole film. After ZIF-67 treatment, the intensity of the Co^{2+} ions increased steeply together with Sn^{2+} ions. The XRD pattern reveals the interface material mainly contains ZIF-67 in Fig. S3. Therefore, the above results proved the ZIF-67 lay between the PTAA and perovskite films.

To further verify the function of ZIF-67 at the PTAA/perovskite interface, we conducted X-ray photoelectron spectroscopy (XPS) patterns and Fourier-transform infrared spectroscopy (FTIR) to provide detailed evidence in Fig. 1(f) and Fig. S4(a). The XPS peak at 399.3 eV was assigned to the N atoms of PTAA and the peak (>400 eV) was attributed to the ZIF-67. Compared to the PTAA film, the XPS peaks from N 1*s* of the PTAA/ZIF-67 sample shifted to the higher binding energy. The fingerprint regions of aromatic C—N stretch vibrations ($\upsilon_{C\text{-}N}$) were the peaks of pristine PTAA at 1316 cm^{-1} [37]. After the ZIF-67 treatment, the peak position shifted to 1320 cm^{-1}. Given these XPS and IR peak shifts, it illustrated that the N atoms of PTAA could interact with the ZIF-67 layer. As shown in Fig. 1(g), the low binding energy peak was identified as N atoms of ZIF-67 and the high binding energy peak was ascribed to N of formamidinium. The fingerprint peak at 1628 cm^{-1} represented C=N stretch vibrations of pure ZIF-67 in Fig. S4(b) [38]. For the ZIF-67/perovskite film, the shifted XPS and IR peak indicated the interaction between the N atoms of ZIF-67 and the perovskite film. The XPS patterns show the high-resolution spectra of the Co 2*p* (Fig. 1h). For the ZIF-67 layer, a characteristic spin or bit splitting of Co 2*p*1/2 peak at 796.9 and Co 2*p*3/2 781.3 eV peak was observed. It also displayed the presence of two intense satellite peaks centered at 802.2 and 785.2 eV. Compared with the pure ZIF-67, the Co peaks of the PTAA/ZIF-67 film shifted to low blinding energy, which verified that the Co element of ZIF-67 had connected with PTAA. The high-resolution spectra of the Pb^{2+} are exhibited (Fig. 1i). Those peaks at 142.8 and 138.0 eV were identified as Pb 4*f*5/2 and Pb 4*f*7/2 in the reference film. After ZIF-67 treatment, the energy shifted toward the low at 142.6 and 137.8 eV. It demonstrated that the interaction indeed existed between ZIF-67 and the Pb^{2+} of the perovskite layer. In short, the Co element in ZIF-67 could coordinate with the N atom of PTAA. Meanwhile, the N atom of the organic functional group interacted with an uncoordinated Pb^{2+} ion in perovskite. Furthermore, the PTAA/ZIF-67 film is more hydrophilic than the pure PTAA film (Fig. S5). The increased hydrophilicity might be attributed to the interface interaction between perovskite or PTAA and ZIF-67. The experimental results coincide with the theoretical calculations quite well.

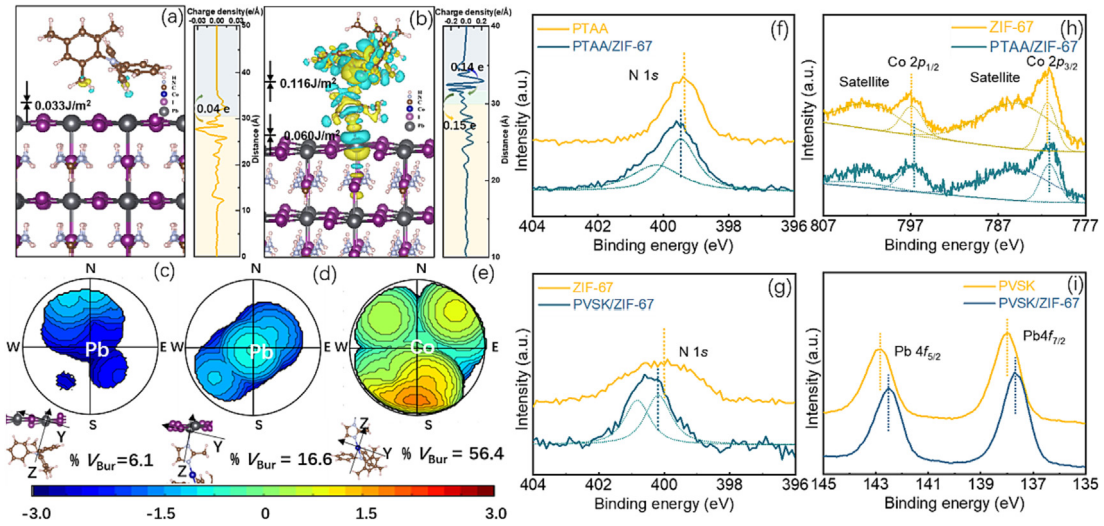

Fig. 1. The charge transfer density difference plots of (a) PTAA/perovskite and (b) PTAA/ZIF-67/perovskite interface, inset: charge density difference coupling with Bader charge analysis; the steric maps of the (c) PTAA/perovskite, (d) ZIF-67/perovskite and (e) PTAA/ZIF-67 interface, insert: the related ball-and-stick representations. High-resolution XPS spectra of N 1*s* of (f) PTAA, PTAA/ZIF-67 film and (g) ZIF-67, perovskite layer with ZIF-67 treatment; high-resolution XPS spectra of (h) Co 2*p* of ZIF-67, PTAA/ZIF-67 layer and (i) Pb 4*f* of perovskite film without and with ZIF-67 treatment.

2.2. Photovoltaic performance

To investigate the influence of the ZIF-67 on the device's photovoltaic performance, we fabricated planar heterojunction solar cells with/without ZIF-67 treatment. Through tuning the concentration of ZIF-67, the best solar cells with 5 mM ZIF-67 were obtained in Fig. S6. As displayed in Fig. 2(a) and Fig. S7, the reference f-PSCs achieved an average power conversion efficiency (PCE) of about 17.8%, with a wide distribution from 16.3% to 18.6%. Through the ZIF-67 treatment, the flexible devices exhibited a higher PCE of around 19.1%, distributed on a narrow range of 18.3% to 20.2%. We also measured the current–density voltage (*J*–*V*) characteristics of the devices by forward and reverse scanning. Compared with the reference, the f-PSCs with ZIF-67 treatment displayed a better PCE of 20.16%, with a short-circuit current density (J_{sc}) of 23.26 mA cm^{-2}, a Fill Factor (FF) of 0.79, an open-circuit voltage (V_{oc}) of 1.10 V in Fig. 2(b). By holding a bias near the maximum power output point (0.92 V), the steady-state efficiency output could be obtained over 19.7% after 200 s illumination, corresponding to a stabilized photocurrent of 21.38 mA cm^{-2} (Insert). Fig. 2(c) exhibits the external quantum efficiency (EQE) spectra of solar cells without and with the ZIF-67 treatment. The integrated photocurrent densities of the flexible devices without and with ZIF-67 were 22.13, and 22.55 mA cm^{-2}, respectively, which was consistent with the J_{sc} derived from the *J*–*V* measurement. Thus, the ZIF-67 treatment is beneficial to the photovoltaic performance, which mainly increases the FF and V_{oc}. The improved photovoltaic parameters may be attributed to the better carrier dynamics at the interface around the absorbing layer as discussed below.

To further explore the mechanisms of the enhanced FF in the f-PSCs, we measured the steady-state photoluminescence spectroscopy (PL) and space-charge-limited current (SCLC) characteristics. Compared with the reference, the ZIF-67-based film with the ITO/PTAA/perovskite structure at the short circuit revealed a lower PL intensity (Fig. S8a). It indicates that the carrier was extracted better from the perovskite absorbent to the hole transport layer by introducing ZIF-67. For the ITO/perovskite/Au devices, the SCLC characteristics demonstrated the carrier mobility increased from 1.28 × 10^{-3} to 1.84 × 10^{-3} cm^2 V^{-1} s^{-1} through the ZIF-67 treatment (Fig. 2d). It showed that the modification interface of ZIF-67 played a critical role in enhancing carrier transport, leading to improved FF.

Through the related calculation, the trap densities of those samples without and with ZIF-67 were 2.104 × 10^{16} and 1.695 × 10^{16} cm^{-3}, respectively. Meanwhile, the PL and time-resolved photoluminescence (TRPL) measurements were carried out. By the ZIF-67 treatment, the films with the glass/perovskite architecture revealed a higher PL intensity in contrast to the reference. The average decay time (τ_{avg}) also increased from 778 to 998 ns in Fig. S8b. The results indicated that the ZIF-67 treatment could reduce the defect density and suppress non-radiative recombination. To understand the mechanism of carrier recombination under open-circuit conditions, the light-intensity-dependent V_{oc} profile was presented in Fig. 2(e). The value of the ideality factor got closer to 2.0, indicating that trap-assisted recombination plays an important role in a solar cell. The devices based on ZIF-67 exhibited a lower ideality factor (1.17) than the reference. It indicates that the ZIF-67 treatment is beneficial for suppressing trap-assisted recombination and reducing defect states, which is the chief reason for the improvement of V_{oc}.

Grazing-incidence wide-angle X-ray scattering (GIWAXS) analysis (Fig. S9) of the perovskite films revealed the crystal orientation was not affected after ZIF treatment [39]. Hence, we rule out the effect of the crystal orientation on carrier transport. To explore the deeper reasons for the improved carrier transport and the decreased interface defects, UV photoelectron spectroscopy was conducted to reveal work function (WF), and valence band maximum (VBM, Fig. 2f and Fig. S10). The VBM of perovskite with ZIF-67 is close to the PTAA. It is to the benefit of the carrier traveling from the perovskite to the PTAA layer. The shift of WF away from the vacuum level indicates the surface becomes more p-type, resulting in the enhanced built-in electric field and the improved charge separation efficiency at the PTAA/perovskite interface [40–42]. With improving the contact between the PTAA and perovskite by ZIF-67 treatment, the defects density at the interface decrease, and carrier transport improves.

2.3. Humidity and light stability

To evaluate the device stability, the normalized PCE was monitored in an air environment (relative humidity: 20%-40%, temper-

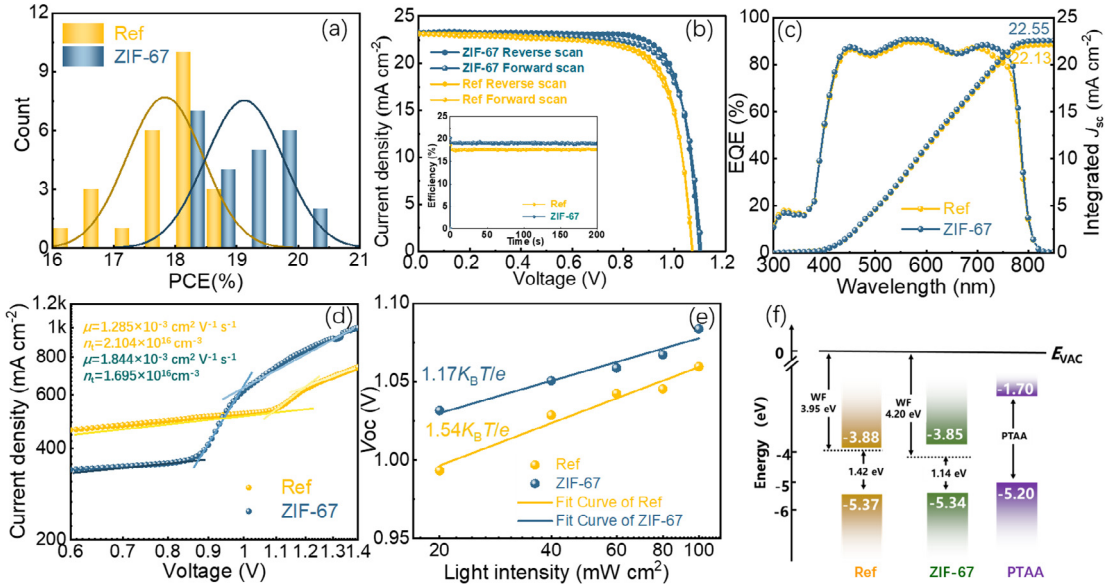

Fig. 2. (a) The histograms. (b) *J–V* curves of the champion solar cells without and with ZIF-67 treatment measured by forward and reverse scan; inset: the steady-state photocurrent measured at a bias voltage (0.88 V for without and 0.92 V with ZIF-67 treatment) near the maximum power point. (c) EQE spectra. (d) SCLC characteristics of the devices with and without ZIF-67 treatment. (e) V_{oc} upon light intensity modulated *J–V* measurements of the devices with and without ZIF-67 treatment. (f) Energy band diagram of ref (left) and ZIF-67 (middle) perovskite films.

ature: 0–10 ℃) at winter, and with continuous light irradiation by a white LED lamp under 1 sun illumination. As shown in Fig. 3(a) and Fig. S11(a-c), the reference devices only kept 55% of their original PCE after 1008 h, while the ZIF-67 modified f-PSCs still maintained 82% of their initial PCE. The open-circuit photo-stability of ZIF-67 modified flexible cells is superior to that of the reference one, maintaining 96% of their original PCE after 1656 h of illumination in Fig. 3(b) and Fig. S11(d-f). Besides, we explore the operational stability of unencapsulated flexible cells under MPP tracking under continuous one-sun irradiation in a nitrogen atmosphere (Fig. 3c). The flexible devices with ZIF-67 retained 80% of their original efficiency over 1200 h, while the efficiencies of the reference cells dropped below 40% in less than 500 h. Due to the diffusion of the electrode at bias, the device without bias exhibited a longer lifetime. In short, the stability test results proved that the incorporation of ZIF-67 enhanced the light stability of flexible devices.

According to the related literature, the decomposition and phase transition in the perovskite film contribute to the PCE degradation under high humidity or intensive light illumination [43]. We performed the XRD and PL mapping measurements to investigate the intrinsic stability of the f-PCSs. From the XRD patterns in Fig. 3(d) and Fig. S12(a-c), only one peak on a scale of 10° to 16° could be observed in the fresh film. This peak was attributed to the diffraction of the (110) lattice plane of the organic–inorganic metal halide perovskite. After the aging treatment of humidity for 62 days, the X-ray diffraction analysis displayed a peak at around 11.9°, assigned to the δ-phase perovskite [44]. The result indicates that a phase transition appeared in the absorber layer. As aging goes on, two additional diffraction peaks appeared at 11.2° and 12.8°, which are possibly assigned to low-dimensional perovskite and PbI_2 [45], respectively. The cause of low-dimensional perovskite was upper interface modification. [46] Compared with the reference films, the samples with ZIF-67 after the same aging had a much lower ratio of inactive phase, including two dimensions, δ-phase, and PbI_2. Based on the above discussion, the perovskite film was made more stable in the high-humidity atmosphere by the ZIF-67 treatment. As indicated in Fig. 3, only the phase transition occurs in the perovskite film upon light irradiation. In Fig. S12(d-f), the evolution trend of the δ-phase perovskite content under continuous sun irradiation was similar to the one in the air environment. However, the rate of phase transition was much slower. Therefore, ZIF-67 also protected the perovskite to delay phase transition under continuous light irradiation.

We investigate the film aging by PL mapping at different aging conditions. Through the variation in peak position over the surface, phase segregation could be clearly observed. The yellow areas correspond to short wavelengths and the violet areas present long wavelengths. As displayed in Fig. 3(f), the PL peak position of fresh perovskite film was around 780 nm. The PL peaks red-shifted after aging at humidity conditions for 75 days. The distribution range of the peak position in the samples with ZIF-67 treatment was narrower than the reference one. As aging goes on, decomposition easily occurs in the reference films. It indicates the ZIF-67 treatment could restrain the film decomposition in a humid environment. After continuous light irradiation for 120 days, the PL peaks in the reference film displayed both the Br-rich (light-green) and I-rich (dark-green) domains (Fig. 3g), wherein the phase separation is more severe in the reference film. It suggests the ZIF-67 treatment prevents the perovskite film from phase separation under continuous light irradiation. Retarded phase separation could increase compositional uniformity and reduce defect concentrations in perovskite film, resulting in improving the device stability [47,48].

We further investigate the residual strain in the film using the tilted angle method [1], to explore the effect of ZIF-67 on the perovskite film degradation. We employed the grazing incident X-ray diffraction (GIXRD) technique in the 500 nm region. Fig. S13 shows the GIXRD peak of the reference with respect to the (012) lattice plane. This lattice plane with a high multiplicity factor could provide accurate analysis of the crystal. Fig. S13 shows the GIXRD peak of the reference with respect is respected to the (012) crystal plane. With the tilted angle ϕ value rising from 10° to 50°, the scattering peaks gradually shifted to the right, implying the decrease of the lattice spacing. As the concentration of ZIF-67 increases, the strain state of the perovskite film changes from strain-free to compressive strain. We could estimate the residual stress of perovskite film without and with 5 mM, 10 mM ZIF-67 to be 1.5, 37.4, and 70.5 MPa, respectively. It is reported the compressive strain could

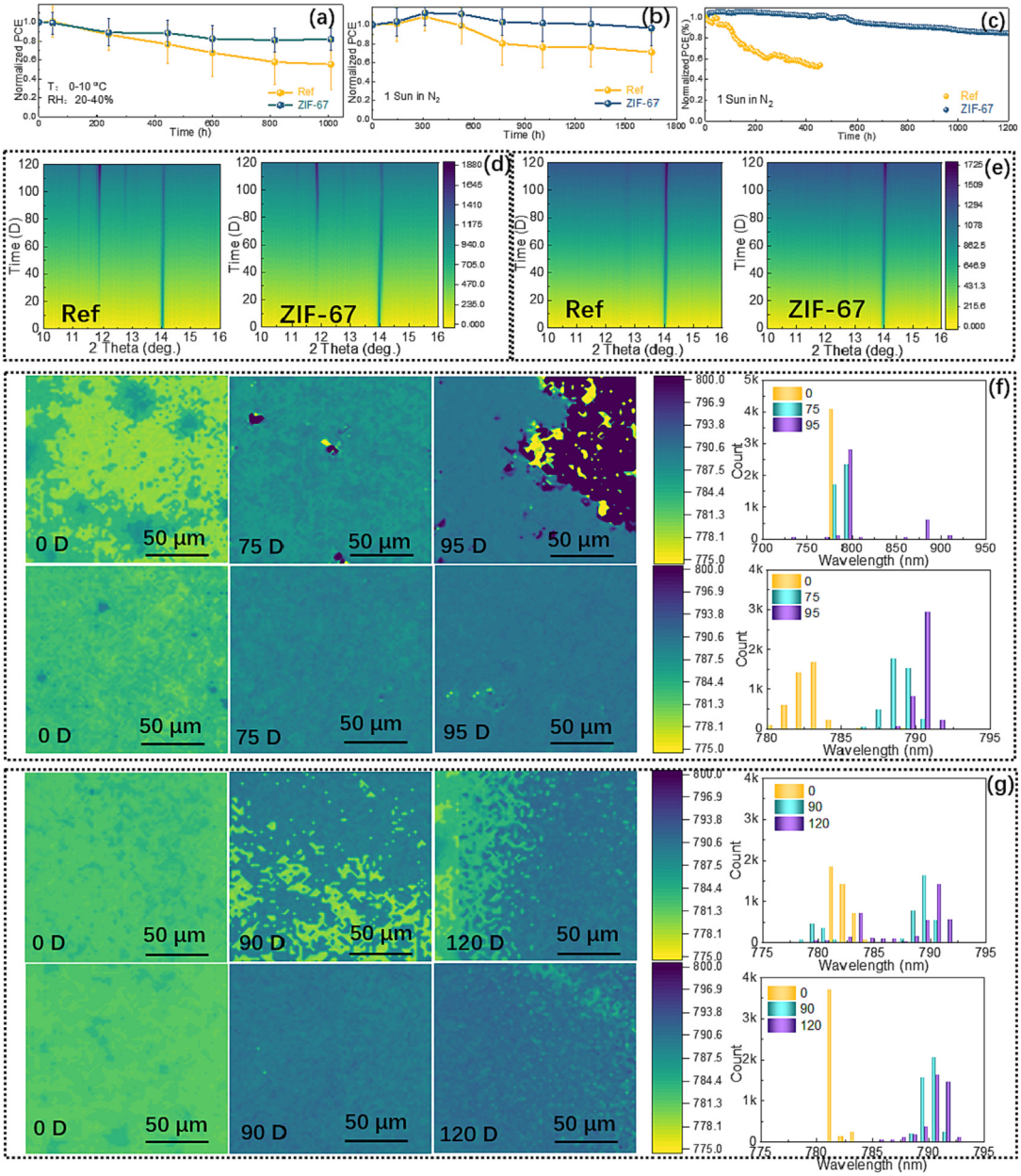

Fig. 3. The PSCs as a function of the storage time in (a) an air environment with a humidity of about 20%–40% at a temperature of about 0–10 ℃ and (b) under continuous light irradiation with 1sun illumination with a white LED lamp. (c) MPP tracking of the device under continuous light irradiation with a white LED lamp, measured at 0.92 V and 1 sun illumination. The contour map of the XRD pattern without and with ZIF-67 treatment. The results are for films maintained (d) with a humidity of about 20%–40% at a temperature of about 0–10 ℃ and (e) upon light irradiation with a white LED lamp under 1 sun illumination. The 2D photoluminescence (PL) maps of perovskite films maintained (f) in air environment with a humidity of about 20%–40% at a temperature of about 0–10 ℃ (upper: REF, under: ZIF-67) and (g) continuous light irradiation with a white LED lamp under 1 sun illumination (upper: REF, under: ZIF-67).

restrict migration, retard vacancy defects, and suppress phase segregation [49]. After ZIF-67 treatment, the close connection of PTAA and perovskite gives rise to compressive strain and fewer defects, leading to the improved humidity and light stability of flexible devices.

2.4. Mechanical stability

For flexible devices, cyclic bending testing is used to evaluate mechanical durability. The efficiency of f-PSC under different radii (from flat to 4 mm) was recorded (Fig. 4a and Fig. S14a–c). The f-PSCs with the ZIF-67 displayed excellent bending resistance. Notedly, the cell without ZIF-67 treatment starts to lose FF under the bending condition of 10 mm because of the perovskite cracking. The values of FF continued to fall until the extreme bending condition of R = 4 mm. As seen in Fig. 4(b) and Fig. S14d-f, the reference cells show a rapid loss of PCE (below 30% of the original PCE after 1000 cycles), while the ZIF-67 modified cell exhibits a long lifetime, retaining over 78% of its initial PCE after 10,000 cycles at R = 6 mm. The decrease in PCE was also attributed to the loss of FF, which was ascribed to perovskite cracking. In Fig. S15, the SEM images showed the obvious mechanical damage cracks in the grains under the bending 1 cycle with different bending radii. These cracks could propagate and even severe crystal shedding could appear with further bending. Compared with the reference, cracks in the perovskite film with ZIF-67 were narrower and shal-

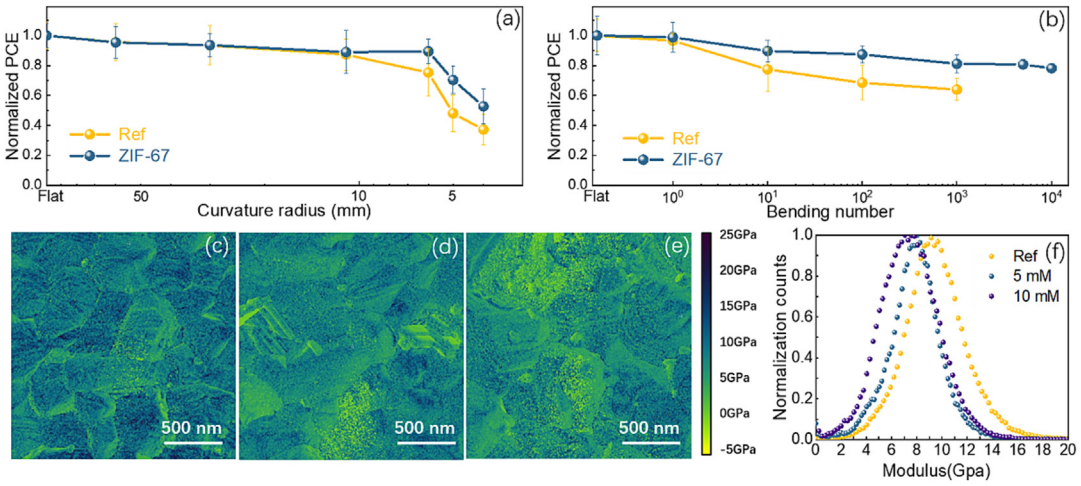

Fig. 4. Efficiency performance of flexible devices (a) under bending 1 cycle with different bending radii and (b) under bending cycles with a radius of 6 mm. Elastic modulus maps of the perovskite films with (c) 0 mM, (d) 5 mM and (e) 10 mM ZIF-67 treatment and (f) the corresponding Young's modulus distribution.

lower. The ZIF-67 treatment makes the perovskite film more difficult to crack, which has a positive effect on improving mechanical stability. As is well known, the cracks increase the resistance by retarding charge transport [50]. Those defects at the interface could serve as the starting points for the development of the cracks [4]. The ZIF-67 modified interface layer could increase the adhesion between the perovskite film and the PTAA layer. It reduced the mechanical defect concentration, which could help to avoid cracking.

In these thin-film solar cells, the perovskite film and transport layer adjacent interact with each other, which influences the bonding strength of metal-halide and the interfacial interaction between different structural subunits and thus the mechanical properties (e.g., nominal elastic modulus) [51]. The peak force quantitative nanoscale mechanical (PF-QNM) atomic force microscopy (AFM) was used to probe the mechanical properties of perovskites film (Fig. 4c–f). Compared with the reference films, the Young's Modulus of the perovskite films with ZIF-67 treatment was reduced from 9.2 to 8.0 GPa. With the increasing concentration of ZIF-67, the Young's Modulus further decreases. These results demonstrated the high resilience of perovskite film was associated with adding ZIF-67, which modifies the film surface with compatible Young's Modulus with PTAA (0.4–4 GPa) [52]. After the ZIF-67 treatment, both the strong adhesiveness at the PTAA/perovskite interface and the high resilience of the perovskite film improved mechanical stability.

3. Conclusions

In conclusion, we provided a simple and effective interfacial modification using ZIF-67, enhancing the efficiency and stability of inverted f-PSCs. The ZIF-67 reinforced the interaction at the interface between PTAA and perovskite. This is favorable for extracting carriers from the perovskite layer and passivating the surface defects. We thus achieved an excellent PCE of 20.16% for the flexible device. Moreover, due to the compressive strain, the ZIF-67 treatment devices maintained 82% of their original PCE after 1200 h with a humidity of 20%–40% and a temperature of 0–10 ℃. Over 1000 h, the f-PSCs based on ZIF-67 interlayer retained 96 and 80% of their original PCE under continuous light irradiation without and with bias, respectively. What's more, owing to the reinforced adhesion, the ZIF-67 treated f-PSCs retained more than 78% of the initial PCE after 10,000 bending cycles. This kind of multifunction material provides a new choice for the further acceleration of its industrialization and may be also applied in the field of light-emitting diodes and other optoelectronics.

Experimental section

Experimental details can be found in the Supporting Information.

Declaration of competing interest

The authors declare that they have no known competing financial interests or personal relationships that could have appeared to influence the work reported in this paper.

Acknowledgments

The authors would like to acknowledge funding support from the National Natural Science Foundation of China (U21A20172, 21975028, 22005035), the Beijing Natural Science Foundation (JQ19008), and the China Postdoctoral Science Foundation (2020M670144, 2020M680012, 2020TQ0043). The authors would like to thank BL14B1in Shanghai Synchrotron Radiation Facility (SSRF) for providing the beam time.

Appendix A. Supplementary data

Supplementary data to this article can be found online at https://doi.org/10.1016/j.jechem.2022.09.044.

References

[1] X. Li, W. Zhang, X. Guo, C. Lu, J. Wei, J. Fang, Science 375 (2022) 434–437.
[2] R. Li, J. Lu, J. Li, T. Yang, A. Amassian, Z. Ding, Y. Chen, S. Liu, W. Huang, Energy Mater. Adv. 2021 (2021) 9671892.
[3] C. Zhu, X. Niu, Y. Fu, N. Li, C. Hu, Y. Chen, X. He, G. Na, P. Liu, H. Zai, Y. Ge, Y. Lu, X. Ke, Y. Bai, S. Yang, P. Chen, Y. Li, M. Sui, L. Zhang, H. Zhou, Q. Chen, Nat. Commun. 10 (2019) 815–826.
[4] H. Wang, C. Zhu, L. Liu, S. Ma, P. Liu, J. Wu, C. Shi, Q. Du, Y. Hao, S. Xiang, H. Chen, P. Chen, Y. Bai, H. Zhou, Y. Li, Q. Chen, Adv. Mater. 31 (2019).
[5] J.H. Heo, D.S. Lee, D.H. Shin, S.H. Im, J. Mater. Chem. A 7 (2019) 888–900.
[6] K.-G. Lim, T.-H. Han, T.-W. Lee, Energy Environ. Sci. 14 (2021) 2009–2035.
[7] G. Lee, M.-C. Kim, Y.W. Choi, N. Ahn, J. Jang, J. Yoon, S.M. Kim, J.-G. Lee, D. Kang, H.S. Jung, M. Choi, Energy Environ. Sci. 12 (2019) 3182–3191.
[8] Y. Hu, T. Niu, Y. Liu, Y. Zhou, Y. Xia, C. Ran, Z. Wu, L. Song, P. Müller-Buschbaum, Y. Chen, W. Huang, ACS Energy Lett. 6 (2021) 2917–2943.
[9] Z. Wu, P. Li, Y. Zhang, Z. Zheng, Small Methods 2 (2018) 1800031.
[10] J. Zhao, Z. Xu, Z. Zhou, S. Xi, Y. Xia, Q. Zhang, L. Huang, L. Mei, Y. Jiang, J. Gao, Z. Zeng, C. Tan, ACS Nano 15 (2021) 10597–10608.

[11] J. Zhang, W. Zhang, H.-M. Cheng, S.R.P. Silva, Mater. Today 39 (2020) 66–88.
[12] S. Wu, Z. Li, J. Zhang, X. Wu, X. Deng, Y. Liu, J. Zhou, C. Zhi, X. Yu, W.C.H. Choy, Z. Zhu, A.K. Jen, Adv. Mater. 33 (2021) 2105539.
[13] X. Wang, K. Rakstys, K. Jack, H. Jin, J. Lai, H. Li, C.S.K. Ranasinghe, J. Saghaei, G. Zhang, P.L. Burn, I.R. Gentle, P.E. Shaw, Nat. Commun. 12 (2021) 52.
[14] L. Zhou, J. Su, Z. Lin, X. Guo, J. Ma, T. Li, J. Zhang, J. Chang, Y. Hao, Energy Mater. Adv. 2021 (2021) 9836752.
[15] Q. Dong, C. Zhu, M. Chen, C. Jiang, J. Guo, Y. Feng, Z. Dai, S.K. Yadavalli, M. Hu, X. Cao, Y. Li, Y. Huang, Z. Liu, Y. Shi, L. Wang, N.P. Padture, Y. Zhou, Nat. Commun. 12 (2021) 973.
[16] Z. Dai, K. Yadavalli Srinivas, M. Chen, A. Abbaspourtamijani, Y. Qi, P. Padture Nitin, Science 372(2021) 618–622.
[17] Q. Dong, M. Chen, Y. Liu, F.T. Eickemeyer, W. Zhao, Z. Dai, Y. Yin, C. Jiang, J. Feng, S. Jin, S. Liu, S.M. Zakeeruddin, M. Grätzel, N.P. Padture, Y. Shi, Joule 5 (2021) 1–15.
[18] Z. Zheng, F. Li, J. Gong, Y. Ma, J. Gu, X. Liu, S. Chen, M. Liu, Adv. Mater. 34 (2022) 2109879.
[19] K. Huang, Y. Peng, Y. Gao, J. Shi, H. Li, X. Mo, H. Huang, Y. Gao, L. Ding, J. Yang, Adv. Energy Mater. 9 (2019) 1901419.
[20] Y. Gao, K. Huang, C. Long, Y. Ding, J. Chang, D. Zhang, L. Etgar, M. Liu, J. Zhang, J. Yang, ACS Energy Lett. 7 (2022) 1412–1445.
[21] C. Long, K. Huang, J. Chang, C. Zuo, Y. Gao, X. Luo, B. Liu, H. Xie, Z. Chen, J. He, H. Huang, Y. Gao, L. Ding, J. Yang, Small 17 (2021) 2102368.
[22] B.L. Watson, N. Rolston, A.D. Printz, R.H. Dauskardt, Energy Environ. Sci. 10 (2017) 2500–2508.
[23] Z. Dai, S.K. Yadavalli, M. Hu, M. Chen, Y. Zhou, N.P. Padture, Scripta Mater. 185 (2020) 47–50.
[24] Q. Zhou, J. Qiu, Y. Wang, M. Yu, J. Liu, X. Zhang, ACS Energy Lett. 6 (2021) 1596–1606.
[25] C. Ge, Z. Yang, X. Liu, Y. Song, A. Wang, Q. Dong, CCS Chem. 3 (2021) 2035–2044.
[26] M. Li, Y.G. Yang, Z.K. Wang, T. Kang, Q. Wang, S.H. Turren-Cruz, X.Y. Gao, C.S. Hsu, L.S. Liao, A. Abate, Adv. Mater. 31 (2019) 1901519.
[27] J.X. Zhong, W.Q. Wu, Y. Zhou, Q. Dong, P. Wang, H. Ma, Z. Wang, C.Y. Yao, X. Chen, G.L. Liu, Y. Shi, D.B. Kuang, Adv. Funct. Mater. 32 (2022) 2200817.
[28] S. Chen, X. Dai, S. Xu, H. Jiao, L. Zhao, J. Huang, Science 373 (2021) 902–907.
[29] L. Yang, J. Feng, Z. Liu, Y. Duan, S. Zhan, S. Yang, K. He, Y. Li, Y. Zhou, N. Yuan, J. Ding, S. Liu, Adv. Mater. 34 (2022) 2201681.
[30] Z. Huang, L. Fan, F. Zhao, B. Chen, K. Xu, S.F. Zhou, J. Zhang, Q. Li, D. Hua, G. Zhan, Adv. Funct. Mater. 29 (2019) 1903774.
[31] W. Zhang, X. Jiang, X. Wang, Y.V. Kaneti, Y. Chen, J. Liu, J.S. Jiang, Y. Yamauchi, M. Hu, Angew. Chem., Int. Ed. 56 (2017) 8435–8440.
[32] G. Zhong, D. Liu, J. Zhang, J. Mater. Chem. A 6 (2018) 1887–1899.
[33] D. Saliba, M. Ammar, M. Rammal, M. Al-Ghoul, M. Hmadeh, J. Am. Chem. Soc. 140 (2018) 1812–1823.
[34] Y. Wang, X. Mei, J. Qiu, Q. Zhou, D. Jia, M. Yu, J. Liu, X. Zhang, J. Phys. Chem. 12 (2021) 11330–11338.
[35] K. Koumpouras, J. A. Larsson, J. Phys.-Condens. Mater. 32 (2020) 315502.
[36] V. Maurya, K.B. Joshi, J Phys. Chem. A 123 (2019) 1999–2007.
[37] T. Ye, W. Chen, S. Jin, S. Hao, X. Zhang, H. Liu, D. He, A.C.S. Appl. Mater. Interfaces 11 (2019) 14004–14010.
[38] Y. Liu, D. Lin, W. Yang, X. An, A. Sun, X. Fan, Q. Pan, Micropor. Mesopor. Mat. 303 (2020) 110304.
[39] Y. Lv, H. Zhang, J. Wang, L. Chen, L. Bian, Z. An, Z. Qian, G. Ren, J. Wu, F. Nüesch, W. Huang, Energy Mater. Adv. 2020 (2020) 2763409.
[40] C. Shi, Q. Song, H. Wang, S. Ma, C. Wang, X. Zhang, J. Dou, T. Song, P. Chen, H. Zhou, Y. Chen, C. Zhu, Y. Bai, Q. Chen, Adv. Funct. Mater. 32 (2022) 2201193.
[41] X. Zheng, Y. Hou, C. Bao, J. Yin, F. Yuan, Z. Huang, K. Song, J. Liu, J. Troughton, N. Gasparini, C. Zhou, Y. Lin, D.-J. Xue, B. Chen, A.K. Johnston, N. Wei, M.N. Hedhili, M. Wei, A.Y. Alsalloum, P. Maity, B. Turedi, C. Yang, D. Baran, T.D. Anthopoulos, Y. Han, Z.-H. Lu, O.F. Mohammed, F. Gao, E.H. Sargent, O.M. Bakr, Nat. Energy 5 (2020) 131–140.
[42] H. Zai, J. Su, C. Zhu, Y. Chen, Y. Ma, P. Zhang, S. Ma, X. Zhang, H. Xie, R. Fan, Z. Huang, N. Li, Y. Zhang, Y. Li, Y. Bai, Z. Gao, X. Wang, J. Hong, K. Sun, J. Chang, H. Zhou, Q. Chen, Joule 5 (2021) 2148–2163.
[43] J. Dou, C. Zhu, H. Wang, Y. Han, S. Ma, X. Niu, N. Li, C. Shi, Z. Qiu, H. Zhou, Y. Bai, Q. Chen, Adv. Mater. 33 (2021) 2102947.
[44] H. Min, M. Kim, S.-U. Lee, H. Kim, G. Kim, K. Choi, J.H. Lee, S.I. Seok, Science 366 (2019) 749.
[45] J.J. Yoo, G. Seo, M.R. Chua, T.G. Park, Y. Lu, F. Rotermund, Y.K. Kim, C.S. Moon, N. J. Jeon, J.P. Correa-Baena, V. Bulovic, S.S. Shin, M.G. Bawendi, J. Seo, Nature 590 (2021) 587–593.
[46] F. H. Isikgor, F. Furlan, J. Liu, E. Ugur, M. K. Eswaran, A. S. Subbiah, E. Yengel, M. De Bastiani, G. T. Harrison, S. Zhumagali, C. T. Howells, E. Aydin, M. Wang, N. Gasparini, T. G. Allen, A. u. Rehman, E. Van Kerschaver, D. Baran, I. McCulloch, T. D. Anthopoulos, U. Schwingenschlögl, F. Laquai, S. De Wolf, Joule 5 (2021) 1566–1586.
[47] S. Ma, Y. Bai, H. Wang, H. Zai, J. Wu, L. Li, S. Xiang, N. Liu, L. Liu, C. Zhu, G. Liu, X. Niu, H. Chen, H. Zhou, Y. Li, Q. Chen, Adv. Energy Mater. 10 (2020) 1902472.
[48] D.J. Slotcavage, H.I. Karunadasa, M.D. McGehee, ACS Energy Lett. 1 (2016) 1199–1205.
[49] L. Wang, Q. Song, F. Pei, Y. Chen, J. Dou, H. Wang, C. Shi, X. Zhang, R. Fan, W. Zhou, Z. Qiu, J. Kang, X. Wang, A. Lambertz, M. Sun, X. Niu, Y. Ma, C. Zhu, H. Zhou, J. Hong, Y. Bai, W. Duan, K. Ding, Q. Chen, Adv. Mater. 34 (2022) 2201315.
[50] H. Liu, Z. Zhang, Z. Su, W. Zuo, Y. Tang, F. Yang, X. Zhang, C. Qin, J. Yang, Z. Li, M. Li, Adv. Sci. 9 (2022) 2105739.
[51] X. Hu, X. Meng, X. Yang, Z. Huang, Z. Xing, P. Li, L. Tan, M. Su, F. Li, Y. Chen, Y. Song, Sci. Bull. 66 (2021) 527–535.
[52] B. Du, O.K.C. Tsui, Q. Zhang, T. He, Langmuir 17 (2001) 3286–3291.